H_2S GAS ADSORPTION STUDIES AND ANTI-BACTERIAL ACTIVITY OF PURE AND MIXED IRON AND NICKEL-MANGANESE OXIDE NANOPARTICLES

S. GUL[a], A. DIN[a], M. I. KHAN[a*], I. UR RAHMAN[b], M. A. KAMBOH[c]
[a]*Department of Chemistry, Kohat University of Science & Technology, Kohat-26000 Khyber Pakhtunkhwa, Pakistan*
[b]*Gandhara College of Pharmacy, Gandhara University, Peshawar, Khyber Pakhtunkhwa, Pakistan.*
[c]*Department of Chemistry, Faculty of Science, Universiti Teknologi Malaysia, Johar Bahru, Malaysia*

In the present work we have presented the synthesis of pure manganese oxide and iron and nickel mixed manganese oxide nanoparticles by using polyol approach. The samples were characterized by FE-SEM, EDS and XRD, size of pure MnO_2 nanoparticles was 5.68 nm and 7.23 & 19.49 nm for Mn-Ni and Mn-Fe nanoparticles respectively. From FE-SEM images average size was calculated for MnO_2 nanoparticles was 91.8 nm, for Mn-Fe 271.55 nm and for Mn-Ni 245.6 nm, showing polydispersity and overlapping of nanoparticles. Anti-bacterial activity against multi-drug-resistant organisms was conducted; adsorption of H_2S gas on the surface of the synthesized nanoparticles was also assayed.

(Received August 6, 2015; Accepted October 2, 2015)

Keywords: Polyol; XRD; EDS; H_2S Adsorption; Anti-bacterial

1. Introduction

Nanomaterials having the size of 1-100 nm have wide applications in the fields of catalysis, optical and electronics devices, biotechnology and environmental sciences due to their extra ordinary characteristics like catalytic, optical, magnetic and anti-bacterial properties than in bulk. A number of pure metal nanoparticles including Fe, Co and Mn, metal oxide such as, CdO, ZnO, Fe_2O_3 and □-Fe_2O_3, alloys such as CoPt, FePt and CoFe and ferrites, such as MFe_2O_4 (M=Cu, Mn, Mg and Ni etc) have been prepared during the last few years due to range of applications in different fields [1-4]. To get morphology and shape control of the nanoparticles during the synthesis, a lot of work has been published during the last few years, introducing new routes and methods of synthesis, like co-precipitation, sole-gel, evaporation method, chemical ultrasonic emulsion method, micro emulsion, electrodeposition, thermal decomposition, Biosynthesis, hydrothermal, chemical reduction and polyol method etc. [5-8].

Magnetic nanoparticles are important due to their applications in the fields of information storage, magnetic refrigeration, controlled drug delivery, medical diagnosis and as ferrofluids [9-12]. Thus, developing new synthetic routes for magnetic nanoparticles and the investigation of their properties are of great importance [13-14].

Among the chemical, physical or electrochemical processes generally used in the particles' production, the most easy and versatile route is the polyol-mediated synthesis of inorganic nanoparticles. Polyols(α-diols and etherglycols) are first recalled in order to explain the versatility of this process. Guidelines which allow controlling the nucleation and growth steps in such media are then given in order to obtain particles with well-defined characteristics namely, a

*Corresponding author: gorikhan@kust.edu.pk

uniform shape, a mean size in the micron, submicron or nanometer range with a narrow size distribution, and a low degree of agglomeration. Examples of size tuning of ferromagnetic metals (Fe, Co, Ni and their alloys) and noble metals are given as well as examples of shape control leading to 1D nanostructures with a particulate emphasis on the growth mechanism of silver nanorods or nanowires. Examples of polyol-mediated synthesis of oxide (spinel ferrites, Cu_2O, ZnO) nanoparticles through hydrolysis reaction are also given [15]. H_2S gas is an air pollutant that is highly toxic even at lower concentrations in the air and also known for causing corrosion; smells like rotten eggs and is colorless. Main sources of H_2S pollution include petroleum industry; according to literature it can be perceived in the air even at 0.002 ppm with the ever-existing risk of fatal intake that may result in respiratory failure. All these facts regarding the synthesis and applications of nanoparticles and environmental issues associated with H_2S gas, we decided to synthesize and evaluate the gas adsorption phenomenon and anti-bacterial potential of the metallic nanoparticles by polyol method.

2. Results and discussion

2.1. XRD

Fig. 1(a), 2(a) and 3(a) showed XRD patterns of manganese oxide and manganese mixed with iron and nickel bimetallic nanoparticles. Particle size was calculated by using Scherrer formula as:

$$D = \frac{k\lambda}{B\cos\theta}$$

Where D is the particle size in nanometers, λ is the wavelength of the radiation (1.5406 Å for CuKα radiation), k is a constant equal to 0.94, B is the corrected peak width at half maximum intensity and θ is the peak position. Size calculated for pure MnO_2 nanoparticles from the most intense peak is 5.68 nm with d spacing equl to 2.48 Å, for Mn-Ni mixed nanoparticles 7.23 nm with d spacing 2.80 Å and for Mn-Fe nanoparticles 19.49 nm with d-spacing equal to 1.21 Å respectively.

2.2. EDS Analysis

For elemental analysis of the synthesized manganese oxide nanoparticles, EDS analysis was performed (Fig. 1(b), 2(b) and 3(b). In MnO_2 nanoparticles, Mn was detected in the range of 5.7-6.1 keV, oxygen at 0.4-0.7 keV and carbon at 0.2-0.4 keV. In Mn-Fe mixed nanoparticle EDS spectra (Fig. 1(b)), Mn was detected in the range of 5.7-6.1 keV, Fe in the range of 6.3-6.6 keV, oxygen at 0.4-0.7 keV, Na at 1.0-1.2 keV and carbon at 0.2-0.4 keV In Mn-Ni mixed nanoparticle EDS spectra (Fig. 2(b)), Mn was detected in the range of 5.7-6.1 keV, Ni in the range of 7.3-7.7 keV, oxygen at 0.4-0.7 keV, Na at 1.0-1.2 keV and Cl at 2.5-2.8 keV and carbon at 0.2-0.4 keV. Cl may arise due to the precursor salt Nickel chloride in Mn-Ni mixed nanoparticles (Fig. 3 (b)).

2.3. FE-SEM

For morphology determination FE-SEM was done; images of all the three types of the synthesized nanoparticles showed agglomeration and polydispersity. Fig. 1 (c) and (d) showed the average particle size for MnO_2 particles was calculated from FE-SEM and associated histogram which was calculated 91.8 nm, for Mn-Fe 273 nm (Fig. 2 (c) and (d)) and for Mn-Ni 246 nm (Fig. 3 (c) and (d)). These calculations are quite different from XRD calculation which showed agglomeration and overlapping of the particles.

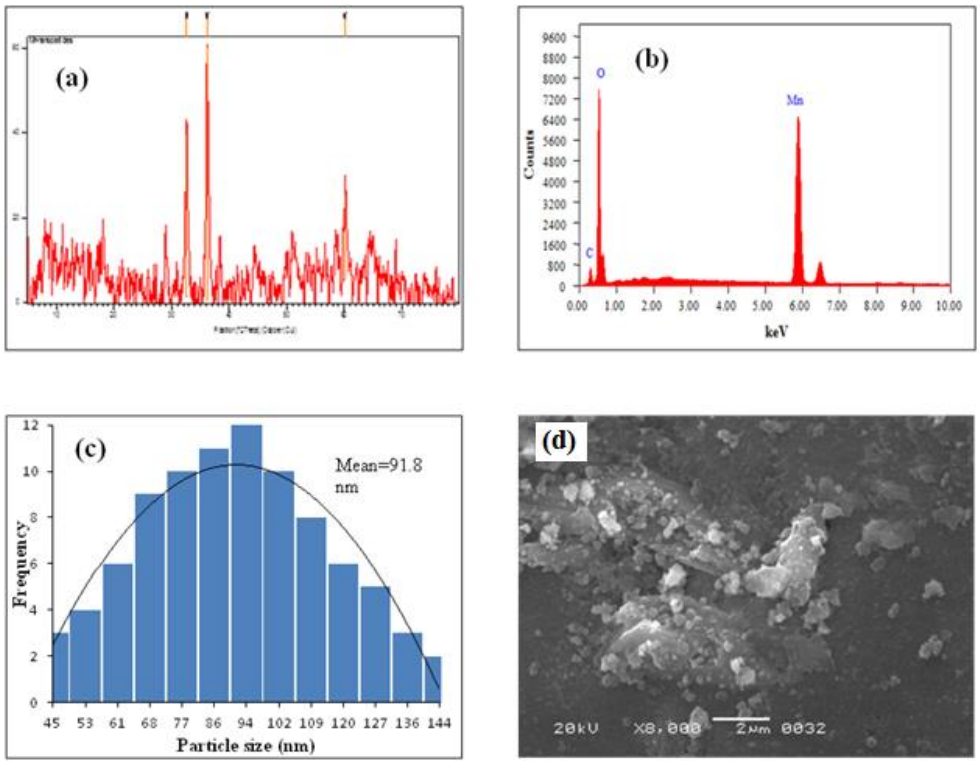

Fig. 1. (a) XRD pattern, (b) EDS, (c) Particle size distribution histogram, (d) FE-SEM image of MnO_2 nanoparticles

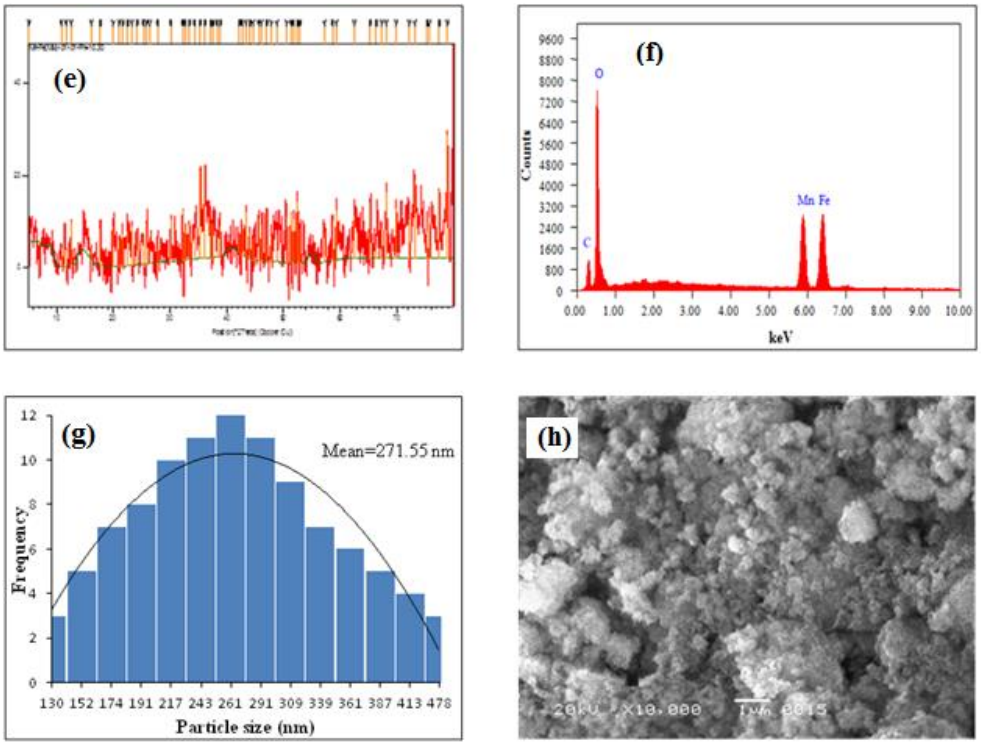

Fig. 2. (a) XRD pattern, (b) EDS, (c) Particle size distribution histogram, (d) FE-SEM image of Mn-Fe nanoparticles

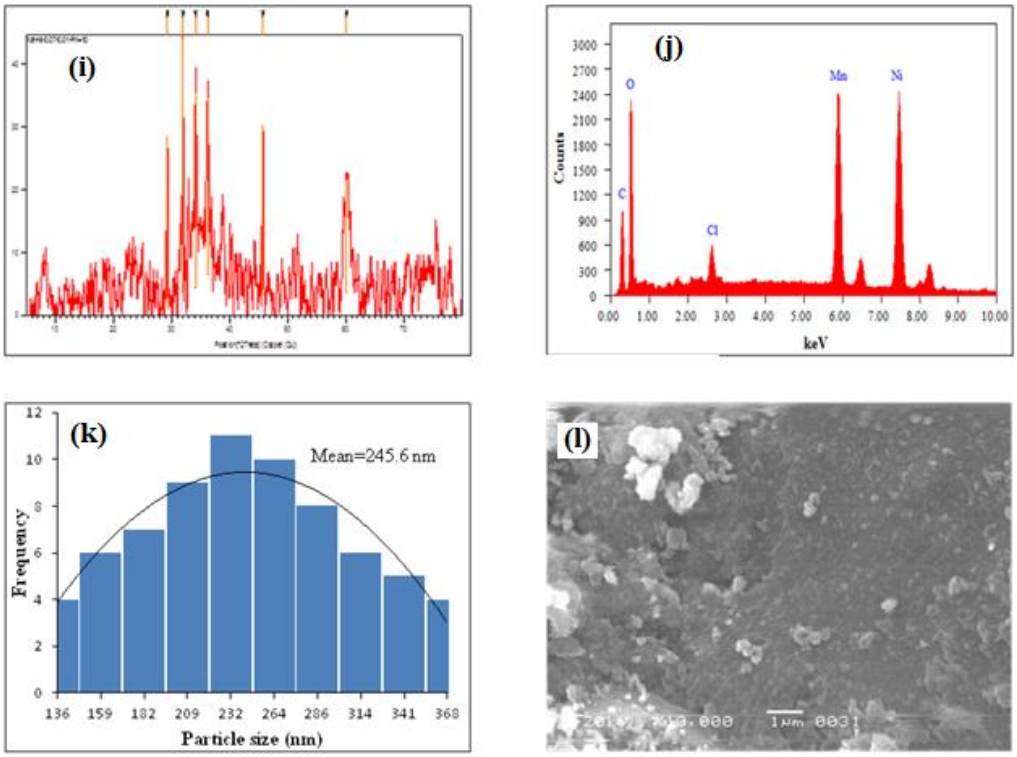

Fig 3. (a) XRD pattern, (b) EDS, (c) Particle size distribution histogram, (d) FE-SEM image of Mn-Ni nanoparticles

2.4. H_2S adsorption study

H_2S gas adsorption capacity of the synthesized nanomaterials was measured as depicted in Fig. 2 and compared with bulk manganese oxide. During the experiment, freshly prepared H_2S was passed through the identical quantities of bulk MnO_2 and synthesized nanomaterials viz. 2.5 g each over a period of 30 min. The extent of adsorption was assessed directly through the time required for change in colour of lead acetate solution from clear solution to black. Bulk manganese oxide blackened the solution within 6 minutes due to the formation of lead sulfide, while synthesized nanomaterials including pure manganese oxide, mixed iron- and nickel-manganese oxide did the same in 25.3, 21.6 and 21.5 minutes respectively with the experiment was pursued as five replicates. The observed increase in elapsed time was due to high surface area to volume ratio was responsible for high surface activity and these features combined to better the degree of adsorption of H_2S in comparison to its bulk manganese oxide.

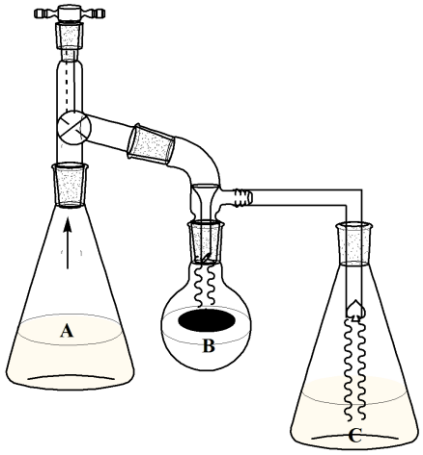

Fig. 2: Assembly for H_2S adsorption study; A: FeS + H_2SO_4 mixture; B: Synthesized nanomaterials powder; C: $Pb(CH_3COO)_2$ solution.

2.5. Anti-bacterial assay

In vitro synergistic effect was assessed by collective anti-bacterial activity of the synthesized nanomaterials and standard antibiotic drug gemifloxacin by disc diffusion assaying protocol against two human pathogens i.e. *staphylococcus aureus* and *escherichia coli* (Table 1). Increase in anti-bacterial effect was calculated by the formula

$$\text{Increase in fold} = \frac{(B^2 - A^2)}{A^2}$$

Where A and B are the zones of inhibition for reference and reference + synthesized nanomaterials respectively; in Table-1, it can be seen that the anti-bacterial activity of gemifloxacin increased when combined with the synthesized nanomaterials against *staphylococcus aureus* as well as *escherichia coli*. Considerable synergistic effect of the synthesized nanomaterials against Gram-positive bacteria and Gram-negative bacteria may be attributed to the interaction of the nanoparticles with the cell walls bacteria as Gram-positive are embedded in double membrane; moreover literature supports an affinity of the metallic nanomaterials towards the cell wall sulfur/phosphorus containing biomolecules [16].

Table-1: Zone of inhibition (mm) of synthesized NPs (8 ppm) and their combined effect against test strains (@ 18 µl/hole); H_2S gas adsorption (minutes).

Material	***S. aureus***	***E. coli***	***Time Elapsed***
Gemifloxacin (A)	16	12	--
MnO_2 NPs	8	9	25.3 (±0.64)
Mn-Fe NPs	6	9	21.6 (±0.77)
Mn-Ni NPs	5	8	21.5 (±0.61)
B = A + MnO_2 NPs (Increase in Fold = $\frac{(B^2 - A^2)}{A^2}$)	22 (0.89)	17 (0.12)	--
B = A + Mn-Fe NPs (Increase in Fold = $\frac{(B^2 - A^2)}{A^2}$)	20 (0.56)	17 (0.12)	--
B = A + Mn-Ni NPs (Increase in Fold = $\frac{(B^2 - A^2)}{A^2}$)	19 (0.41)	18 (0.26)	--
Bulk MnO_2	--	--	4 (±0.64)

3. Experimental

Analytical grade manganese sulphate, iron sulphate and nickel chloride were supplied by BDH, sodium hydroxide, ethylene glycol and acetone were purchased from Merck and were used without further purification.

3.1. Characterization of the nanoparticles

Morphology and average size of prepared nanoparticles were determined by field emission-scanning electron microscope (FE-SEM), JEOL (JSM-7600F, Japan). For elemental analysis energy dispersive X-rays spectrometry was performed using oxford-EDS system from JEOL (JSM-7600F, Japan). The prepared nanoparticles were analyzed by ARLTM ARLX'TRA Powder Diffractometer with Cu Kα radiation (α =1.540 56 Å), and the operation voltage 40 kV and current 250 mA.

3.2. Preparation of manganese oxide nanoparticles

10 mL of double distilled water was mixed with 20 mL ethylene glycol following by mixing of 70 mL 0.1 M manganese sulphate solution and kept for stirring for 30 minutes. pH of the transparent reaction mixture was adjusted at 10.3 using digital pH meter by adding hydrazine hydrate solution drop wise, altering the colour of the solution to dark brown. Reaction mixture was refluxed for 4 hours along with constant stirring; cooled to room temperature giving cloudy brown particles, which were separated by centrifugation followed by washing five times with acetone and annealing at 150 ºC for 5 hours.

3.3. Preparation of manganese-iron bimetallic nanoparticles

20 mL of ethylene glycol was mixed with 10 mL of double distilled water and 35 mL 0.1 M solutions of each manganese sulphate and iron sulphate solutions and adjusted the pH of the reaction mixture at 10 monitored by digital pH-meter by drop wise addition of hydrazine hydrate solution. The reaction mixture was then refluxed for 5 hours and cooled to room temperature; black particles were separated by centrifugation; washed with acetone four times to remove the impurities and annealed at 200 °C for 4 hours.

3.4. Preparation of manganese-nickel bimetallic nanoparticles

10 mL of double distilled water was mixed with 20 mL ethylene glycol following by mixing of 35 mL of 0.01 M Nickel and 35 mL of 0.07 M of manganese sulphate solutions in it and pH of the solution was adjusted to 10 by adding hydrazine hydrate solution, turning the colour of the mixture from colourless to brown; refluxed for 3 hours, brown particles were separated by centrifugation, followed by washing three times with acetone and annealed at 200 °C for 4 hours.

3.5. H_2S adsorption study

In our lab, we have established a setup for the assessment of adsorption capacity of the synthesized materials (Fig. 2). In flask A, H_2S gas was generated by the reaction of iron sulfide and sulphuric acid; the gas was flown to flask B containing solid material (2.5 g) for adsorption phenomenon for one hour; after completion of adsorption the extra gas was purged into flask C containing lead acetate solution. Adsorption capacity was assessed by measurement of time elapsed in minutes taken to change in the colour of the lead acetate solution to black due to the formation of lead sulfide.

3.6. Anti-bacterial assay

Disk diffusion method was used for the anti-bacterial activity of the synthesized nanoparticles, against *Staphylococcus aureus* (Gram-positive) and *Escherichia coli* (Gram-negative); gemifloxacin was used as reference drug and all experiments were conducted in triplicate.

4. Conclusions

We have successfully synthesized pure MnO_2 and Ni & Fe-mixed nanomaterials by polyol method. These proved to be efficient adsorbents for H_2S gas, which in turn can effectively remove H_2S from acid gases produced during industrial processes. We also conclude that the chemically synthesized nanomaterials are potent anti-bacterial agents and can be used in environmental monitoring systems, water purification, biomedical research etc. At the same time, waste generated during synthesis of nanoparticles may be very dangerous because of their size; consequently before the application of these materials as medicines and in environmental devices, it is emphasized to extend their study further.

References

[1] S. Ramesh, B. C. Sekhar, P. S. V. S. Rao and B. P. Rao, Ceramics International **40**, 8729 (2014).
[2] E. R. kumar, R. Jayaprakash and R. Patel, Superlattices and Microstructures, **62**, 277 (2013).
[3] M. Zheng, X. C. Wu, B. S. Zou and Y. J. Wang, Journal of Magnetism and Magnetic Material, **183**, 152 (1998).
[4] S. M. El-Refaei, M. I. Awad, B. E. El-Anadouli and M. M. Saleh, Electrochimica Acta, **62**, 277 (2013).
[5] S. S. Waghmare, A. M. Deshmukh, S. W. Kulkarni and L. A. Oswaldo, Universal Journal of Environmental Research and Technology, **1**, 64 (2011).
[6] V. S. Kalyamwar, F. C. Raghuwanshi, N. L. Jadhao and A. J. Gadewar, Journal of Sensor Technology, **3**, 31 (2013).
[7] M. Faraji, Y. Yamini and M. Razaee, Journal of the Iranian Chemical Society, **7**, 1 (2010).
[8] Z. Ying, J. Shengming, Q. Guanzhou and Y. Min, Materials Science and Engineering: B, **122**, 222 (2005).
[9] T. M. Bhave, C. Balasubramanian, H. Nagar, S. Kulkarni, R. Pasricha, P. P. Bakare, S.K. Date and S. V. Bhoraskar, Hyperfine Interactions, **160**, 199 (2005).
[10] R. D. McMichael, R. D. Shull, L. J. Swartzendruber and L. H. Bennett, Journal of Magnetism and Magnetic Materials, **111**, 29 (1992).
[11] S. P. Bhatnagar and R. E. Rosensweig, Journal of Magnetism and Magnetic Materials, **149**, 198 (1995).
[12] L. Josephson, C. H. Tung, A. Moore and R. Weissleder, Bioconjugate Chemistry **10**, 186 (1999).
[13] M. Zahn, Journal of Magnetism and Magnetic Materials **85**, 181 (1990).
[14] K. V. P. M. Shafi, A. Ulman, A. Dyal, X. Yan N. L. Yang, C. Estournes, L. Fournes, A. Wattiaux, H. White and M. Rafailovich, Chemistry of Materials, **14**, 1778 (2002).
[15] R. Brayner, F. Fievet and T. Coradin, In Nanomaterials: A Danger or a Promise? A Chemical and Biological Prospective, Springer-Verlag, London (2013).
[16] R.K. Kunkalekar, M.M. Naik, S.K. Duey and A.V. Salker, Journal of Chemical Technology and Biotechnology, **88**, 873 (2013).